ChemComm

Synthesis of Mo and Ru solid-solution alloy NPs and their hydrogen evolution reaction activity

Journal:	*ChemComm*
Manuscript ID	CC-COM-09-2020-005958.R1
Article Type:	Communication

COMMUNICATION

Synthesis of Mo and Ru solid-solution alloy NPs and their hydrogen evolution reaction activity

Received 00th January 20xx,
Accepted 00th January 20xx

DOI: 10.1039/x0xx00000x

Shinya Okazoe[a], Kohei Kusada[a,*], Dongshuang Wu[a], Tomokazu Yamamoto[b,c], Takaaki Toriyama[c], Syo Matsumura[b,c], Shogo Kawaguchi[d], Yoshiki Kubota[e] and Hiroshi Kitagawa [a,*]

We report the synthesis of MoRu solid-solution alloy nanoparticles using carbonyl complexes as a precursor through thermal decomposition. Alloying Ru with an early transition metal, Mo, leads to the electronic structure change, resulting in the enhancement of the catalytic activity for hydrogen evolution reaction, which overtook the Pt catalyst.

The platinum group metals (PGMs) are known as an efficient catalyst for various reactions.[1,2] Although their properties are quite attractive, their usage needs to be reduced because they are not abundant elements on Earth.

One of the ways of enhancing the catalytic properties is using them as nanoparticles (NPs) having a high surface-to-volume ratio. In addition, alloying, which allows fine tuning of the electronic structures of catalysts is also explored, with the aim of improving the catalytic properties further. For example, Pt–Ir,[3] Pt–Ru,[4] Au–Ir,[5] Ag–Ir,[6] Au–Ru,[7] Pd–Ru,[8] Ir–Cu,[9] Ru–Ni,[10,11] and Ru–Cu[12] solid-solution NPs were synthesized by bottom-up methods such as liquid-phase reduction, and PGMs' catalytic properties were improved. However, most of the PGM-based solid-solution alloy NPs involved combinations with late transition metals, and there are fewer reports with early transition metals. Although there are some reports with solid-solution alloy NPs such as Pt–Mn,[13] Pt–Cr,[14] and Rh–W,[15] alloying PGMs with early transition metals is still a challenging task due to their large negative redox potentials.

In this communication, we report on the simple synthesis of NPs made of a MoRu solid-solution alloy. Ru is the cheapest metal among PGMs, and Ru also shows high catalytic properties. For instance, among the PGMs Ru shows a relatively higher hydrogen evolution reaction (HER) performance.[16] In the Mo–Ru system there are miscible regions in both rich compositions in the bulk,[17] but there are few reports on MoRu solid-solution NPs.[18,19] Here, we focused on the thermal decomposition of zero-valent carbonyl metal complexes. The obtained NPs were characterized by scanning transmission electron microscopy (STEM), energy dispersive X-ray (EDX) spectroscopy, and synchrotron powder X-ray diffraction (PXRD) analysis. Furthermore, the HER performance of the synthesized MoRu solid-solution alloy NPs was investigated. We confirmed a large enhancement of HER activity compared with Ru NPs.

For the synthesis of MoRu solid-solution alloy NPs, both molybdenum hexacarbonyl ($Mo(CO)_6$) and triruthenium dodecacarbonyl ($Ru_3(CO)_{12}$) were added to oleylamine as a solvent and stabilizing agent, and then the solution was heated to 330 °C under magnetic stirring for 2 h under nitrogen gas flow. The prepared NPs were separated by centrifugation using hexane and acetone. The synthetic details are shown in ESI.

STEM-EDX analyses were performed to obtain direct evidence of the formation of a solid-solution structure. A high-angle annular dark-field (HAADF)-STEM image, the corresponding Mo-L and Ru-L EDX maps and an overlay of Mo and Ru maps are shown in Fig. 1a–d. They clearly show that the Mo and Ru atoms are randomly distributed in each NP. In addition, from the EDX result, the ratio of Mo to Ru was calculated to be 0.15:0.85, which was consistent with the X-ray fluorescence spectroscopy result. We further characterized the MoRu NPs by EDX line scanning analysis (Fig. 1e, f). The direction of the line scan is denoted by an arrow across the NP in Fig. 1e. This result also shows that Mo and Ru atoms are distributed over the whole particle. These results indicate the formation of MoRu solid-solution alloy NPs.

We investigated the crystal structure of the NPs using an atomic resolution STEM. Typical examples of HAADF-STEM images are shown in Fig 2. A hexagonal atomic arrangement corresponding to a hexagonal close-packed (hcp) lattice viewed along the [001] direction is shown in Fig. 2a. The lattice spacing of (1–10) was calculated to be 2.3 Å. An atomic arrangement of a face-centred cubic (fcc) structure (ABCABC… stacking sequence of close-packed planes) was also observed (Fig. 2b), and its (111) lattice spacing was calculated to be 2.3 Å. These

[a] Division of Chemistry, Graduate School of Science, Kyoto University, Kitashirakawa-Oiwakecho, Sakyo-ku, Kyoto 606-8502, Japan.
[b] Department of Applied Quantum Physics and Nuclear Engineering, Kyushu University, 744 Motooka, Nishi-ku, Fukuoka 819-0395, Japan.
[c] The Ultramicroscopy Research Center, Kyushu University, Motooka 744, Nishi-ku, Fukuoka 819-0395, Japan.
[d] Japan Synchrotron Radiation Research Insitute (JASRI), SPring-8, 1-1-1 Kouto, Sayo-cho, Sayo-gun, Hyogo 679-5198, Japan.
[e] Department of Physical Science, Graduate School of Science, Osaka Prefecture University, Sakai, Osaka 599-8531, Japan.
†Electronic Supplementary Information (ESI) available: Experimental methods and materials, tables and figures. See DOI: 10.1039/x0xx00000x

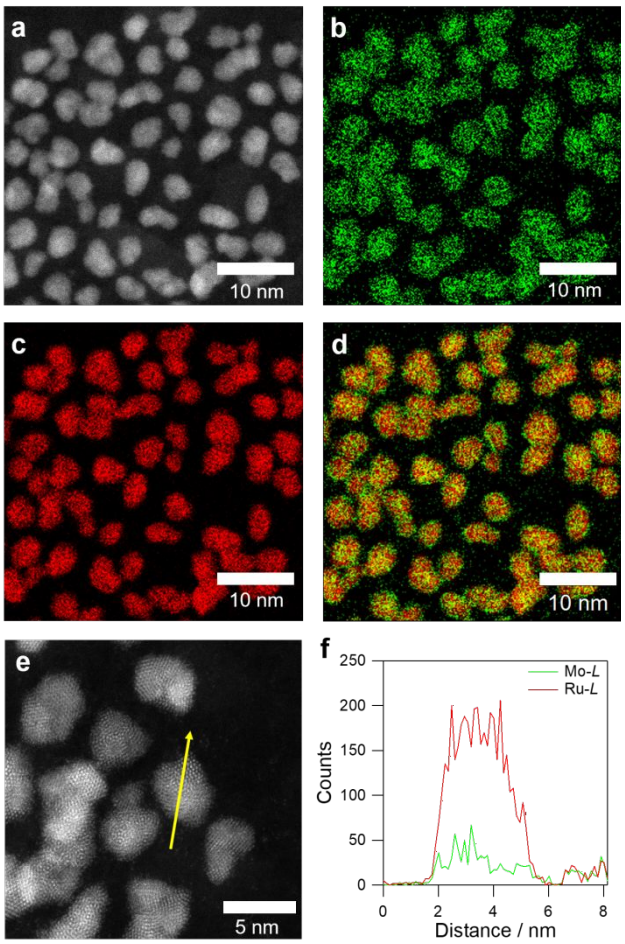

Fig. 1 **a** HAADF-STEM image of MoRu NPs. STEM-EDX maps of **b** Mo-*L* and **c** Ru-*L*. **d** Overlay image of **(b)** and **(c)**. **e** HAADF-STEM image of MoRu NPs. **f** EDX line profile of a MoRu NP along the arrow shown in **(e)**. Mo-*L* and Ru-*L* are indicated as green and red lines, respectively.

results showed that the synthesized MoRu NPs consist of both hcp and fcc structures.

To further study the crystal structure of the synthesized NPs, the PXRD pattern was analysed by Rietveld refinement (Fig. 3a). The best fit revealed that the NPs consist mainly of a hcp phase (76%) with the lattice constants of 2.7882(7) and 4.3716(9) Å for a_{hcp} and c_{hcp} (Table S1, 2), and the remainder (24%) is a fcc phase with 3.8560(7) Å. The atomic arrangements of the hcp structure along the [001] direction and the fcc structure along the [–110] direction were simulated using lattice constants obtained by Rietveld refinements (Fig. 3b, c). The lattice spacings of hcp (1–10) and fcc (111) estimated by the reconstruction using the results of Rietveld refinement almost agreed with the observed values in Fig. 2a, b.

The lattice constants calculated by Rietveld refinement of the MoRu alloy NPs are larger than Ru NPs synthesized by the liquid phase reduction (Fig. S1, Table S3) and the reported values of Ru (hcp Ru (a = 2.7058 Å, c = 4.2819 Å, PDF #00-006-0663), fcc Ru (a = 3.83 Å, PDF #01-088-2333)). Considering the atomic radii of Mo and Ru, the calculated lattice constants of MoRu NPs are slightly larger than the ideal values (Fig. S2). This would be

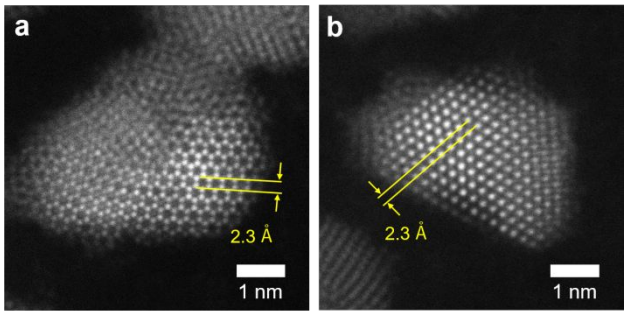

Fig. 2 Atomic resolution HAADF-STEM images of MoRu NPs. **a** A hexagonal structure corresponding to an hcp structure viewed along the [001] direction. **b** ABCABC… stacking of close-packed planes corresponding to a fcc structure viewed in the [–110] direction.

caused by the insertion of carbon atoms to the interstitial sites of hcp and fcc lattice during the synthesis because Mo tends to form carbide easily.[20] Although Ru has only hcp structure in bulk, it was reported that Ru NPs can form fcc structure through bottom-up method using a specific Ru precursor.[21] In addition, *in-situ* XAS revealed that the ligand of precursor stabilized fcc (111) facet. Therefore, by taking advantage of the stabilization of surface energy, fcc structure is preferentially formed rather than hcp structure in $Ru(acac)_3$ solution.[22] We synthesized Ru NPs using the same method as MoRu NPs and found that the Ru NPs were composed of hcp and fcc structures (Fig. S3, Table. S4, 5). Carbonyl ligand may play a similar role to acetylacetonate (acac). Therefore, the MoRu NPs formed both hcp and fcc structures.

To obtain the further evidence of solid-solution alloy structure formation, we measured XPS spectra. When Mo and Ru atoms are mixed at the atomic level, charge transfer from Mo to Ru would occur due to the larger electron negativity of Ru. As shown in Fig. S4, Ru 3*p* peaks of MoRu NPs shifted to slightly lower energy compared to those of bulk Ru (Table S6). On the other hand, Mo 3*d* peaks showed opposite tendency (Table S7). This result revealed the charge transfer from Mo to Ru and further supported the formation of solid-solution alloy structure.

We investigated the catalytic activity for an alkaline HER using the synthesized MoRu solid-solution alloy NPs with a standard three-electrode system. The synthesized MoRu NPs and Ru NPs synthesized by liquid phase reduction and thermal decomposition were loaded onto Vulcan XC 72R carbon at 20 wt% metal and washed with acetic acid before electrochemical tests to remove extra surfactant and expose the catalytically active surface.[23,24] The MoRu NPs supported on the carbon (MoRu/C) maintained the solid-solution structure even after acetic acid washing as shown by STEM-EDX map and line analysis (Fig S5, 6). 20 wt% Pt/C (commercial) was also investigated as a reference. TEM images of NPs and catalysts, and their mean diameters are shown in Fig S7–14 and Table S8. The Mo/C catalyst synthesized by the same method as the MoRu solid-solution alloy NPs showed negligible HER catalytic activity (Fig. S16). We compared the activities by overpotentials

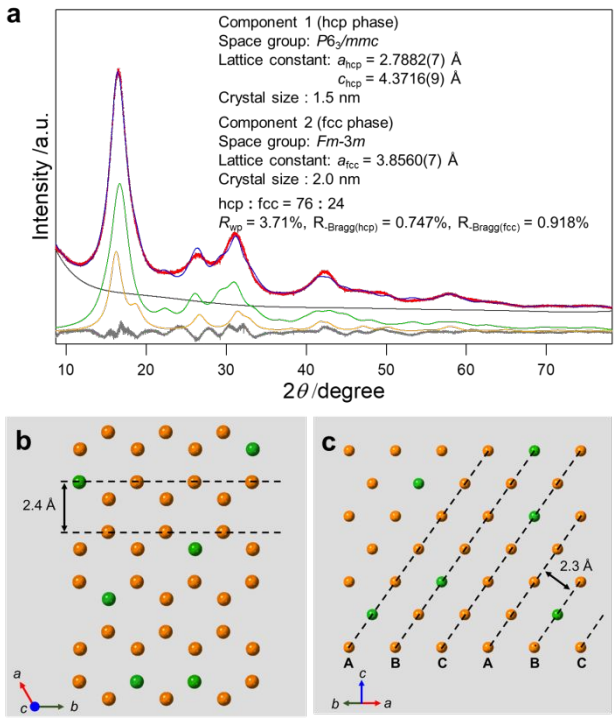

Fig. 3 **a** Synchrotron XRD analysis of MoRu solid-solution alloy NPs at room temperature, 2θ = 8.70 to 78.21 degrees. The radiation wavelength was 0.62921(4) Å. The diffraction pattern is shown as red dots. The calculated pattern is shown as the blue line. The difference profile, the background and fitting curves of hcp and fcc components are shown as grey, black, green, and yellow lines, respectively. **b** Model for the atomic arrangement of the hcp structure viewed along [001]. **c** Model for the atomic arrangement of the fcc structure viewed along the [–110] using the calculated lattice constants by Rietveld refinement.

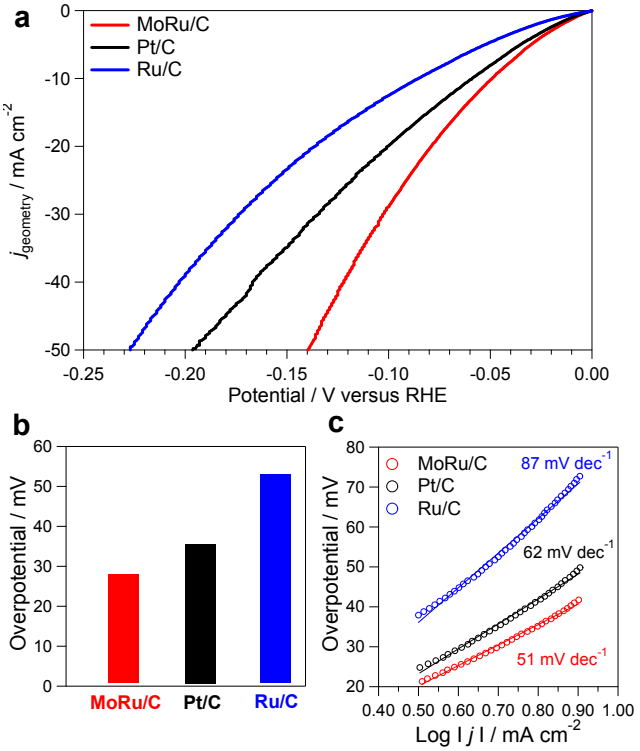

Fig. 4 **a** Polarization curves of 20 wt% catalysts in 1.0 M KOH solution. **b** Overpotentials at –5 mA cm^{-2} (geometry). **c** Tafel plot.

and Tafel plots (Fig. 4a–c) for the almost same size of MoRu/C, Ru/C synthesized by the liquid phase reduction and Pt/C. The overpotentials at –5 mA cm^{-2} are 27.1 mV (MoRu/C), 35.1 mV (Pt/C), 52.5 mV (Ru/C), and 62.4 mV (Ru/C synthesized by the thermal decomposition) (Fig. 4b and S18).

The synthesized MoRu/C showed the best HER catalytic activity. The current density normalized by the electrochemically active surface area (ECSA) was also calculated to make a fair comparison on the HER activity of the catalysts (Fig. S19). The ECSA values of MoRu/C, Pt/C, and Ru/C were 113.31, 82.47, and 96.69 m^2 g^{-1}, respectively (see Table S9). ECSA-normalized polarization curves are shown in Fig. S20. In the lower overpotential region (~–80 mV), the MoRu/C and Pt/C catalysts showed comparable activities. However, MoRu/C showed a higher activity over –80 mV than Pt/C. These results suggest that the catalytic activity of Ru was enhanced by alloying Ru with Mo at the atomic level. The Tafel slopes of MoRu/C, Pt/C, and Ru/C are 51, 62, and 87 mV dec^{-1}, respectively (Fig. 4c). MoRu/C showed the smallest Tafel slope. In an alkaline solution, HER consists of the following three steps.[25]

(Volmer step) $H_2O + e^- + * \rightarrow H^* + OH^-$
(Heyrovsky step) $H_2O + e^- + H^* \rightarrow H_2 + OH^-$
(Tafel step) $2H^* \rightarrow H_2$

A rate-determining step (RDS) of HER can be estimated by the value of the Tafel slope. Around 120 mV dec^{-1}, the RDS is considered to be a Volmer step, namely, a water dissociation process. By contrast, around 40 mV dec^{-1} was considered to be a hydrogen production process (Heyrovsky step). The Tafel slope of Pt/C corresponded to that of previous reports,[26] and the RDS was considered as a Heyrovsky step.[27] The RDS of MoRu/C is also considered as a Heyrovsky step, the same as Pt/C.

Furthermore, we examined the stability of MoRu/C by the chronoamperometry (Fig.S21). Although the mean diameter of MoRu NPs did not significantly change (from 2.6 ± 0.4 nm to 2.7 ± 0.5 nm), their morphology slightly changed, (Fig. S22), which implies surface reconstruction occurred during the HER test. We further directly investigated this structural change by STEM-EDX line analysis. As shown in Fig. S23, we confirmed that the intensity of Mo-*K* line near the particle surface decreased after the stability test. These results showed that Mo leached from the surface of MoRu NPs. XPS spectra before and after stability test also supported Mo dissolution (Fig. S4, Table S6) because Mo signal were not clearly observed after the stability test. Consequently, although the HER activity of MoRu/C after the stability test become slightly lower than the before stability test, it was comparable to Pt/C as shown in Fig. S24.The electronic structure of a catalyst plays a significant role in determining catalytic behaviour.[28] The HER activity strongly relates to the hydrogen adsorption energy. As the hydrogen adsorption energy on the catalyst surface depends on the electronic structure of the catalyst, the HER activity can be controlled by tuning the electronic structure of the catalyst through the

formation of a solid-solution alloy.[29] Ru has a larger d-band centre and stronger hydrogen adsorption energy than Pt.[30, 31] Since the charge transfer from Mo to Ru occurs in the MoRu solid-solution alloy NPs, the hydrogen adsorption energy on Ru sites could be weakened, resulting in the enhancement of Ru HER activity.

In summary, we successfully synthesized MoRu solid-solution alloy NPs by a simple thermal decomposition method. Synchrotron PXRD analysis and STEM-EDX map corroborated the formation of the solid-solution alloy structure. The synthesized MoRu NPs showed an HER activity superior to monometallic Ru NPs. This result suggests that solid-solution alloying of PGMs with an early transition metal is significant for tuning the electronic states and developing new catalysts. However, since the present MoRu catalyst does not have enough high stability, the improvement of its stability is needed.

This work was supported by ACCEL from the Japan Science and Technology Agency (JST), Grant Number JPMJAC1501, and JSPS KAKENHI Grant Number 19J15102, Japan. Synchrotron PXRD measurements were conducted at BL02B2 in SPring-8 with the approval of the Japan Synchrotron Radiation Research Institute (JASRI) (proposal No. 2019B1143). STEM observations were performed as part of a program conducted by the Advanced Characterization Nanotechnology Platform sponsored by The Ministry of Education, Culture, Sports, Science and Technology (MEXT), Japan.

Conflicts of interest

There are no conflicts to declare.

Notes and references

1. J. P. Boitiaux, J. Cosyns and E. Robert, *Appl. Catal.*, 1987, **35**, 193–209.
2. J. A. Don and J. J. F. Scholten, *Faraday Discuss. Chem. Soc.*, 1981, **72**, 145–156.
3. T. Zhang, S. C. Li, W. Zhu, Z. P. Zhang, J. Gu and Y. W. Zhang, *Nanoscale*, 2017, **9**, 1154–1165.
4. D. Strmcnik, M. Uchimura, C. Wang, R. Subbaraman, N. Danilovic, D. van der Vliet, A. P. Paulikas, V. R. Stamenkovic and N. M. Markovic, *Nat. Chem.*, 2013, **5**, 300–306.
5. K. Kusada, D. Wu, T. Yamamoto, T. Toriyama, S. Matsumura, W. Xie, M. Koyama, S. Kawaguchi, Y. Kubota and H. Kitagawa, *Chem. Sci.*, 2019, **10**, 652–656.
6. H. Guo, H. Li, K. Jarvis, H. Wan, P. Kunal, S. G. Dunning, Y. Liu, G. Henkelman and S. M. Humphrey, *ACS Catal.*, 2018, **8**, 11386–11397.
7. Q. Zhang, K. Kusada, D. Wu, N. Ogiwara, T. Yamamoto, T. Toriyama, S. Matsumura, S. Kawaguchi, Y. Kubota, T. Honma and H. Kitagawa, *Chem. Sci.*, 2019, **10**, 5133–5137.
8. K. Kusada, H. Kobayashi, R. Ikeda, Y. Kubota, M. Takata, S. Toh, T. Yamamoto, S. Matsumura, N. Sumi, K. Sato, K. Nagaoka and H. Kitagawa, *J. Am. Chem. Soc.*, 2014, **136**, 1864–1871.
9. F. Wang, K. Kusada, D. Wu, T. Yamamoto, T. Toriyama, S. Matsumura, Y. Nanba, M. Koyama and H. Kitagawa, *Angew. Chem. Int. Ed. Engl.*, 2018, **57**, 4505–4509.
10. K. Mori, K. Miyawaki and H. Yamashita, *ACS Catal.*, 2016, **6**, 3128–3135.
11. J. Zhang, J. Teo, X. Chen, H. Asakura, T. Tanaka, K. Teramura and N. Yan, *ACS Catal.*, 2014, **4**, 1574–1583.
12. B. Huang, H. Kobayashi, T. Yamamoto, S. Matsumura, Y. Nishida, K. Sato, K. Nagaoka, S. Kawaguchi, Y. Kubota and H. Kitagawa, *J. Am. Chem. Soc.*, 2017, **139**, 4643–4646.
13. Y. Kang and B. C. Murray, *J. Am. Chem. Soc.*, 2010, **132**, 7568–7569.
14. H. Yang, N. Vante, J. Le´ger and C. Lamy, *J. Phys. Chem. B*, 2004, **108**, 1938–1947.
15. W. Zhang, L. Wang, H. Liu, Y. Hao, H. Li, M. U. Khan and J. Zeng, *Nano Lett.*, 2017, **17**, 788–793.
16. D. Wu, K. Kusada, T. Yamamoto, T. Toriyama, S. Matsumura, I. Gueye, O. Seo, J. Kim, S. Hiroi, O. Sakata, S. Kawaguchi, Y. Kubota and H. Kitagawa, *Chem. Sci.*, 2020, *in press*
17. E. Anderson and W. H. Rohtery, *J. Less Common Met.*, 1960, **2**, 443–450.
18. G. Beamson, A. J. Papworth, C. Philipps, A. M. Smith and R. Whyman, *Adv. Synth. Catal.*, 2010, **352**, 869–883.
19. S. Liu, C. Chen, Y. Zhang, Q. Zheng, S. Zhang, X. Mu, C. Chen, J. Ma and S. Mu, *J. Mater. Chem. A*, 2019, **7**, 14466–14472.
20. A. M. Gómez-Marín, J. L. Bott-Neto, J. B. Souza, T. L. Silva, W. Beck, L. C. Varanda and E. A. Ticianelli, *ChemElectroChem*, 2016, **3**, 1570–1579.
21. K. Kusada, H. Kobayashi, T. Yamamoto, S. Matsumura, N. Sumi, K. Sato, K. Nagaoka, Y. Kubota, H. Kitagawa*, J. Am. Chem. Soc.,* 2013, **135**, 5493–5496
22. N. Araki, K. Kusada, S. Yoshioka, T. Sugiyama, T. Ina, H. Kitagawa, *Chem. Lett.,* 2019, **48**, 1062–1064
23. D. Li, C. Wang, D. Tripkovic, S. Sun, N. M. Markovic and V. R. Stamenkovic, *ACS Catal.*, 2012, **2**, 1358–1362.
24. V. Mazumder and S. Sun, *J. Am. Chem. Soc.*, 2009, **131**, 4588–4589.
25. T. Shinagawa, A. T. Garcia-Esparza and K. Takanabe, *Sci. Rep.*, 2015, **5**, 13801.
26. L. Lin, Z. Sun, M. Yuan, J. He, R. Long, H. Li, C. Nan, G. Sun and S. Ma, *J. Mater. Chem. A*, 2018, **6**, 8068–8077.
27. B. Wang, Z. Wang, X. Wang, B. Zheng, W. Zhang and Y. Chen, *J. Mater. Chem. A*, 2018, **6**, 12701–12707.
28. B. Hammer and J. K. Norskov, *Nature*, 1995, **376**, 238–240.
29. A. Nairan, P. Zou, C. Liang, J. Liu, D. Wu, P. Liu and C. Yang, *Adv. Funct. Mat.*, 2019, **29**, 1903747.
30. A. Vojvodic, J. K. Nørskov and F. Abild-Pedersen, *Topics in Catalysis*, 2013, **57**, 25–32.
31. L. Kristinsdóttir and E. Skúlason, *Surf. Sci.*, 2012, **606**, 1400–1404.

